Predictive Control Based on Ranking Multi-objective Optimization Approaches for a quasi-Z Source Inverter

Abualkasim Bakeer, *Student Member, IEEE*, Gaber Magdy, Andrii Chub, *Senior Member, IEEE*, and Dmitri Vinnikov, *Senior Member, IEEE*

***Abstract*—In power converter control, predictive control has several merits, such as simple concept and fast response. However, the necessity to use the weighting factor inside the cost function makes the control design complex in the case of regulating multi-variables where the value of the weighting factor is obtained by a nontrivial process. Also, it primarily depends on the system parameters and operating points of the control system. This paper aims to enhance the model predictive algorithm of the single-stage topology of a quasi-Z Source Inverter (qZSI). The concept of a multi-objective optimization approach is used in addition to the sub-cost function definition to remove the weighting factors. By using the sub-cost function definition, the inductor current is pushed away from the main loop of the predictive algorithm. Thus, no weighting factor is needed to manage the priority of the inductor current. The other two control targets, which are the capacitor voltage and load currents, will be controlled by the multi-objective optimization approach without using any weighting factors. A detailed theoretical analysis of the proposed technique will be given and validated based on simulation results.**

***Index Terms*—Cost function definition, model predictive control, optimization methods, quasi-Z Source Inverter (qZSI), weighting factors.**

I. Introduction

SHORT-CIRCUITS across a DC source, due to simultaneous gating of upper and bottom switches of the phase leg and the availability of only a buck function, are the main limitations of the traditional voltage source inverter (VSI). The open-circuit and the voltage boost function are the clear obstacles for the current source inverter (CSI). However, along with the fast developments in this research area, a new inverter topology has been proposed by Professor F. Z. Peng to solve the above-mentioned limitations related to traditional VSI and CSI [1]–[4]. The proposed topology, called a Z-Source Inverter (ZSI), is shown in Fig. 1.

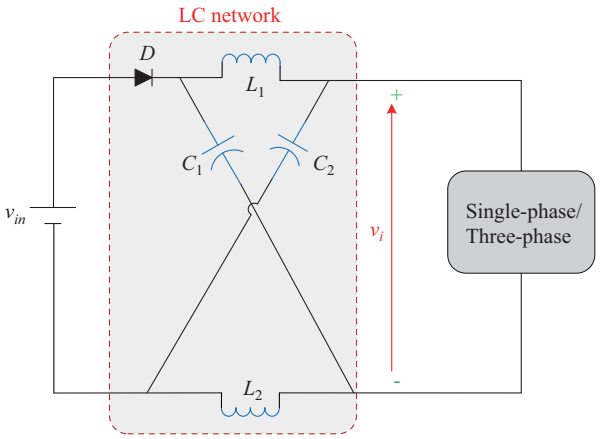

Fig. 1. Basic Z-Source Inverter topology.

This topology contains passive elements (L, C) in its configuration, which are arranged in X-shape and connected to the DC-source through a diode at the front connection. The basic principle of ZSI is achieved by applying the shoot-through state that is attained at shorting the load terminals. Consequently, ZSI utilizes the zero state in the traditional actuation patterns of VSI to raise the input voltage to the desired level. ZSI is a promising topology with the buck-boost functionality within a single-stage without using more semiconductors.

Since its appearance in the research community, ZSI has been addressed in numerous papers to enhance its overall characteristics [2], [3]. These papers focus on the trends in the ZSI family targeted at developing new topologies to improve the step-up features and minimize the voltage stress of the elements [5], [6]. New pulse-width modulation (PWM) techniques for generating the shoot-through states that are used to boost the input voltage have been studied [7], [8]. Another trend is the control of the ZSI that has two main goals: first, to control the DC-part that extends from the input voltage into the DC-link of ZSI, where both the voltage across

Manuscript received April 20, 2020; revised June 25, 2020; accepted October 25, 2020. Date of online publication December 21, 2020; date of current version August 23, 2021. This work was supported in part by the Estonian Research Council grant PUT1443, and in part by the Estonian Centre of Excellence in Zero Energy and Resource Efficient Smart Buildings and Districts, ZEBE, grant 2014-2020.4.01.15-0016 funded by the European Regional Development Fund.

A. Bakeer (corresponding author, email: abualkasim.bakeer@aswu.edu.eg) is with the Department of Electrical Engineering, Faculty of Engineering, Aswan University, 81542 Aswan, Egypt, and also with the Power Electronics Group, Department of Electrical Power Engineering and Mechatronics, Tallinn University of Technology, Tallinn 19086, Estonia.

G. Magdy is with the Department of Electrical Engineering, Faculty of Energy Engineering, Aswan University, 81542 Aswan, Egypt.

A. Chub and D. Vinnikov are with the Power Electronics Group, Department of Electrical Power Engineering and Mechatronics, Tallinn University of Technology, Tallinn 19086, Estonia.

DOI: 10.17775/CSEEJPES.2020.01310

the capacitor and the current in the inductor are controlled; second, to control the AC-part that is similar to the control of the traditional VSI, which is the current or the voltage control mode [9], [10]. Among ZSI-derived topologies, the quasi ZSI (qZSI) looks most promising as it features the reduced capacitor voltage stress and continuous input current using similar component counts as in the basic ZSI [11] shown in Fig. 2.

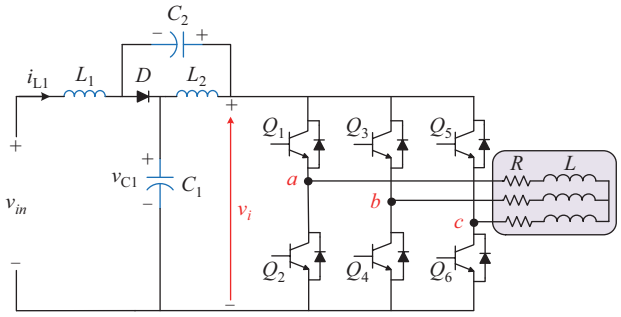

Fig. 2. Configuration of the qZSI.

For any system, the control stage has a pivotal role to realize the desired aim of the system. This area has been studied intensively [12]. In recent years, predictive control is becoming more popular in different applications. The class of model predictive control (MPC) has been developed in the field of power electronics since the 1980 s thanks to the microprocessor revolution of digital boards, such as digital signal processors (DSPs). Thus, the sampling time can have lower values for fast speed implementation [12]–[16]. This new controller has been evaluated against the conventional control methods, such as the PID controller; the results show that predictive control has a higher dynamics response than the PID controller [17], [18]. The main reason for the fast response by MPC depends on the actuation of the converter switches obtained from a future point of view. Future behavior of the variables is acquired using their discrete model at the various switching states of the converter.

This paper begins with a short review of papers addressing the predictive controller within the ZSI/qZSI family. An algorithm is presented for the design of the predictive control for the qZSI without any weighting factor to simplify the control design. This can be achieved by applying the procedure of the sub-cost function definition with the inductor current that is pushed away from the main loop of the predictive algorithm. The multi-objective optimization based on a ranking approach for the capacitor voltage and the three-phase output currents is used to avoid using the weighting factors with these control objectives. The remainder of this paper is organized as follows: Section II discusses previous algorithms of MPC with ZSI/qZSI. Section III introduces the discrete model for qZSI control objectives, and Section IV analyzes in detail the proposed MPC algorithm. Section V shows the simulation results to validate the algorithm based on different tests. Finally, the conclusions are presented in Section VI.

II. Model Predictive Control with ZSI Family

A. General Description

Finite Control Set-MPC (FCS-MPC) has several advantages for power converter control. Its concept depends on the discrete nature of switches, easy implementation, and fast response of the variables. Fig. 3 shows a pattern of how the predictive control attempts to track the reference value of a controlled variable, i.e., the inductor current $i_{\mathrm{L}}(kT)$, where T is the sampling interval.

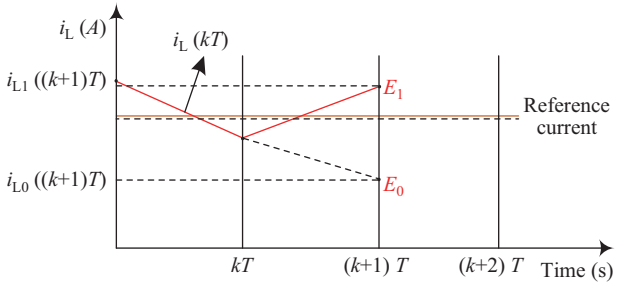

Fig. 3. Illustration of inductor current prediction methodology.

If the topology that includes the inductor has only one switch, the inductor current has two future values, which are $i_{\mathrm{L0}}\left((k+1)T\right)$ and $i_{\mathrm{L1}}\left((k+1)T\right)$ when the status of the switch is either in turn-off or turn-on, respectively. These future values are calculated according to the inductor discrete model relative to the circuit structure. Consequently, it is very important to set an accurate model for the variables under control. The absolute deviation among the reference current and that predicted at turning-on the switch is E_1, while at turning-off the switch is E_0. As shown in Fig. 3, E_1 has a smaller value than E_0. Hence, the optimized state for the converter would happen at turning-on the converter switch in the next sampling time. By applying this state, the inductor current is approaching its reference value. Using the same principle, the optimized state is chosen according to the minimum objective function if there are more than two states. At a greater number of control goals, the weighting factor will be used for each control variable to satisfy their desirable performance. The value of each weighting factor is obtained through a complex tuning process. Consequently, it would be reasonable to avoid the selection process of these weighting factors.

B. MPC for ZSI Family

ZSI class has a unique switching state, i.e., the shoot-through state, at which the input voltage could be boosted. In the DC-side, which starts from the input voltage, v_{in}, untile the DC-link voltage, v_i, the purpose of the control stage is to retain the DC-link voltage fixed at a predefined value to avoid the stress across the switching devices and also to ensure the normal operation of the converter (ZSI/qZSI). The capacitor voltage, $v_{\mathrm{C_1}}$, is considered an easy method to achieve this target, where the peak value of the DC-link voltage is difficult to detect because it needs external hardware circuits. Thus, control complexity and cost may be increased [19]. The DC-side in ZSI/qZSI has the non-minimum phase criteria as

ZSI/qZSI has a zero in the right half-plane. This makes the control design challenging and limited. For this reason, to control the capacitor voltage, the inductor current has to be controlled. In the AC-side of the inverter, either current or voltage control direction is the main requirement.

In 2011, the utilization of MPC with the Z-Source power converter was initiated [20]. In this paper, the discrete model for the inductor current as well as the capacitor voltage was developed for the first time. The paper reports the simulation results for the output current and the output voltage control. The main cost function contains either the current or the voltage control mode, inductor current, capacitor voltage, and switching frequency. Furthermore, the authors refer to the zero state to minimize the effect of the non-minimum phase due to the right half-plane (RHP) in the converter model. Some researchers do not take the null state as an extra term in the cost function because it is already included in the loop, i.e., the optimization loop has eight cycles. Although this paper introduced voltage control using MPC for ZSI, it was not shown how it can be achieved with the studied converter of ZSI.

Then in [21], the control of ZSI with multilevel inverters as a neutral point clamped inverter were examined based on the MPC, and the theoretical analysis for the proposed control approach was confirmed only with the simulation results. The same authors in [20], [21] used MPC with ZSI to obtain the maximum power from the photovoltaic (PV) modules with variations in the irradiation, which was followed by the injection of the captured power to the utility grid [22]. No strategy was proposed on how to achieve the maximum power and how the shoot-through state can be inserted in the design of the possible switching states of the inverter. More importantly, the absolute error for the current control in the cost function has the same value at applying the null state and the shoot-through state. Consequently, the current control is not in charge of selecting the shoot-through state that gives the boosting feature for the impedance converter.

MPC has been employed with another modified topology from the ZSI family, which is quasi ZSI due to its clear merits over ZSI. In [23], the discrete model for the capacitor voltage and the output currents was designed with the application of standalone RL load. The proposed cost function included the output current term without a weighting factor and a term for the capacitor voltage with a weighting factor. A real-time implementation for the proposed control was given based on dSPACE-1103. Five sensors were required for the feedback signals: three current sensors for the load currents, a voltage sensor for the capacitor voltage detection, and a current sensor for the inductor current. The input DC-source is assumed to be constant during the design of the control. The presented results did not show the waveform of the inductor current despite its vital role in checking the stability of the control system. Within the same topology of qZSI, the FCS-MPC was used as a powerful control method for the grid connection in [24], [25]. The cost function included an extra term for the inductor current. Then the parallel algorithm of the FCS-MPC with qZSI aimed to exploit the parallel processing feature of the FPGA digital board [26], [27].

The parallel algorithm can reduce the computational power and overcome overrun limitations. Experimental results are given for the controlled items at a single operating point. In [28], the bidirectional qZSI was used to feed the induction motor, and the torque of the induction motor was controlled by the predictive control. The proposed cost function consisted of the torque term, flux control term, and the capacitor voltage term. The feedback signals were the inductor current, capacitor voltage, the currents of two phases from the stator of the machine (assumption of the balanced case), and the speed of the motor. The error between the reference speed and the actual speed is regulated by the linear controller based on the PI controller to generate the reference value for the machine torque. Based on the measurements of the AC currents, the flux of the stator and the rotor was calculated. According to the minimum cost function, the switching signals for the switches were generated. The authors only validated the proposed algorithm through a simulation study.

The authors in [29] utilized FCS-MPC for another topology in the ZSI family, which is a switched-inductor qZSI. The paper introduces the aims of the discrete model of control according to the topology configuration. In this paper, the relationship of the voltage between the two capacitors (C_1, C_2) is used to avoid measuring the voltage across C_2 to calculate the future inductor current. The proposed control was validated based on the simulation and experimental waveforms. The same authors have proposed an algorithm for FCS-MPC with qZSI circuit with a lower number of sensors [30]. Here, the sensor of the inductor current is removed and its value is obtained through a proposed estimation methodology. This methodology depends on the previous applied optimized state of qZSI and the capacitor voltage during this state. The control system has been confirmed by using simulation results. The same authors have proposed an FCS-MPC algorithm for qZSI in which the objective function has only one weighting factor for the capacitor voltage and its validation is based on the simulation and experimental results [31], [32].

The title of the paper [33] refers to the use of the grid connection with PV but the results presented lack this use. In [34], [35], direct MPC is compared with the linear PWM scheme of the PI in the qZSI topology. Then, the predictive control is used with single-phase qZSI to solve the problem of power decoupling with experimental validation in [36]. FCS-MPC is used with four-leg qZSI to control the load currents at both balanced and unbalanced load conditions with the simulation and experimental confirmations [37]–[39].

III. FCS-MPC Discrete Modeling with qZSI

As mentioned previously, building the FCS-MPC starts with identifying the discrete model of the control goals during different switching states. The discrete model for the control objectives is the same as in [26], [31].

A. Three-phase Load Currents

The load current is one of the control objects, so the actual three-phase currents will be measured as feedback signals into the control block, as shown in Fig. 4. These signals are

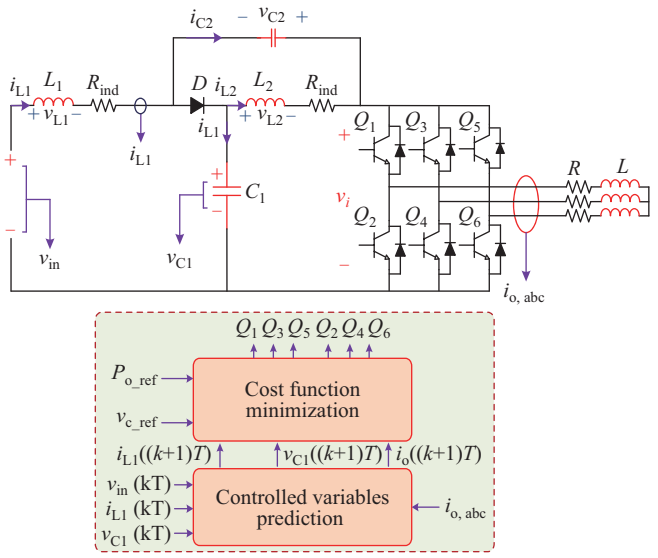

Fig. 4. Overall FCS-MPC strategy for qZSI with a standalone RL system.

transformed into stationary frames (α, β), resulting in two components instead of three. The three-phase inverter has six switched devices (Q_1: Q_6) with possible eight switching states, as listed in Table I. The space vectors of the inverter output voltage across the load terminals during the eight switching states are sketched in Fig. 5. In general, for the ZSI family, the eight switching states could be divided into two states as active states (V_1: V_6) and shoot-through state (V_7).

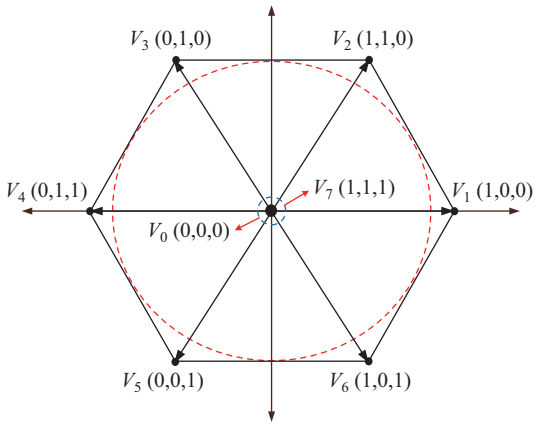

Fig. 5. Space vectors of qZSI output voltage at load terminals.

The value of the future output current $i_o((k+1)T)$ by which the trajectory of the load current could be predicted, is given as:

$$i_o\left((k+1)T\right) = \frac{TV_x\left((k+1)T\right) + Li_o(kT)}{L + RT} \tag{1}$$

where $V_x\left((k+1)T\right)$ is the space vector of qZSI output voltage at the inverter terminals ($V_0 : V_7$) in (α, β) coordinate system as in (2), x is the number of the state signal vectors in Table I, $x \in [0:7]$, $i_o(kT)$ is the actual load currents that include two components in (α, β), T is the sampling interval, R and L are the resistance and inductance of the standalone RL load, respectively.

TABLE I
SWITCHING STATES OF QZS

x	V_x	Q_1	Q_2	Q_3	Q_4	Q_5	Q_6
0	V_0	0	0	0	1	1	1
1	V_1	1	0	0	0	1	1
2	V_2	1	1	0	0	0	1
3	V_3	0	1	0	1	0	1
4	V_4	0	1	1	1	0	0
5	V_5	0	0	1	1	1	0
6	V_6	1	0	1	0	1	0
7	V_7	1	1	1	1	1	1

$$V_x\left((k+1)T\right) = \frac{2}{3}V_{dc}(Q_1 + aQ_2 + a^2Q_3) \tag{2}$$

where V_{dc} is the maximum value of the DC-link voltage, which equals $(2v_{in}(k) - v_{C1}(k))$ and $v_{in}(k)$ is the input source.

The reference load current is computed based on the desired load power (P_{o_ref}) as follows:

$$i_o^*\left((k+1)T\right) = 1.414\sqrt{\frac{P_{o\_ref}}{3R}} \tag{3}$$

B. Inductor Current and Capacitor Voltage

These control variables have different discrete models according to the switching state of the converter.

1) Non Shoot-through Case

The simplified circuit of qZSI during this state is depicted in Fig. 6. It includes the number of states as $x \in [0:6]$. The inductor current in the future $i_{L1}((k+1)T)$ and the future capacitor voltage $v_{C_1}((k+1)T)$ during this case can be given as:

$$i_{L1}\left((k+1)T\right) = \frac{T(v_{in}(kT) - v_{C_1}(kT)) + L_1 i_{L1}(kT)}{L_1 + R_{ind}\cdot T} \tag{4}$$

$$v_{C_1}\left((k+1)T\right) = v_{C_1}(kT) + \frac{T}{C_1}\left(i_{L1}\left((k+1)T\right) - i_{inv}\left((k+1)T\right)\right) \tag{5}$$

where R_{ind} is the parasitic resistance (ESR) of the qZS network inductor, L_1 and C_1 are the inductance and capacitance values of the qZSI LC network, respectively.

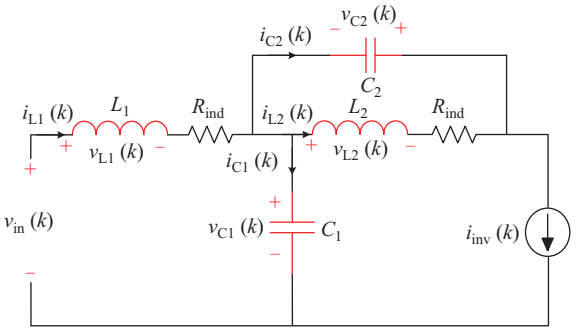

Fig. 6. qZSI circuit in the non shoot-through case.

2) Shoot-through Case

The equivalent circuit of qZSI during this state is shown in Fig. 7. The discrete model inductor current and capacitor voltage, in this case, can be determined as:

$$i_{L1}\left((k+1)T\right) = \frac{Tv_{C_1}(kT) + L_1 i_{L1}(kT)}{L_1 + R_{ind}T} \tag{6}$$

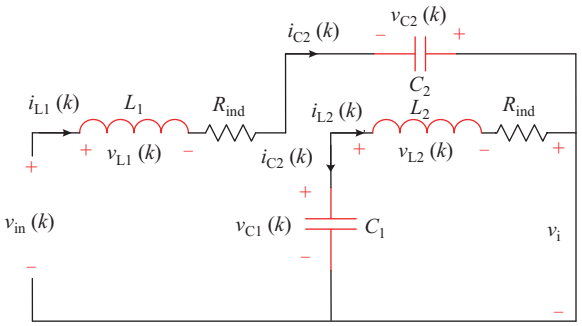

Fig. 7. qZSI circuit in the shoot-through case.

$$v_{C_1}((k+1)T) = v_{C_1}(kT) - \frac{T}{C_1} i_{L1}((k+1)T) \tag{7}$$

IV. Proposed Algorithm for FCS-MPC of qZSI

The proposed algorithm uses the same discrete model of the control objectives as stated above. It primarily contains two definitions.

A. Sub-cost Function Definition

The inductor current has been removed from the main cost function and pushed outside the main loop of the control algorithm. Consequently, the main loop will control both the capacitor voltage and the load currents. This loop contains the active states of the converter, $x \in [0:6]$. Despite the inductor current being removed from the main loop, it will be controlled by the sub-cost function before executing the main loop. The inductor current is considered a key factor to control the capacitor voltage where it is the only control objective that decides the shoot-through case.

The flowchart of the proposed sub-cost function is sketched in Fig. 8. The sub-cost function at non shoot-through g_{ns} is calculated by subtracting the reference inductor current and the predicted one at the non shoot-through case. The same procedure is applied with the shoot-through cost function g_s, but with the predicted inductor current at the shoot-through case. After that, if the minimum cost function is at the shoot-through case, then the shoot-though vector is applied directly to the converter switches without the need to check the other

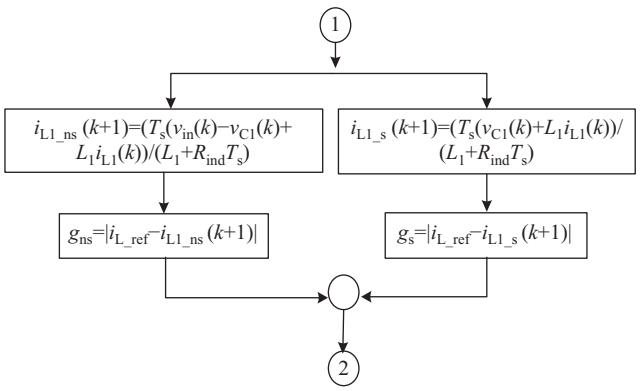

Fig. 8. Calculations of the sub-cost function.

seven states. Otherwise, if the non shoot-through case gives the minimum sub-cost function, the algorithm must check the other states inside the main loop to select one of the seven states that have the minimum cost function. However, there is no need to calculate the future capacitor voltage at the shoot-through case. Choosing the shoot-through from the beginning of the algorithm without passing through the main loop reduces the number of calculations.

As mentioned above, the inductor current calculations are computed before the main calculation loop. In the capacitor voltage prediction at shoot-through, it is not essential to use the proposed algorithm for the calculation. The prediction of the capacitor voltage during active states uses the prediction value for the inductor current at active states that is calculated in the sub-cost function part.

B. Multi-objective Optimization Ranking Definition

As the cost function in the previous algorithms has more than one term in its formula, it is essential to use the weighting factor [40]. The multi-objective optimization approach aims at minimizing the following two cost functions:

$$g_{\text{vC1}}(x) = |v_{C1\_ref}((k+1)T) - v_{\text{C1}}((k+1)T)| \tag{8}$$

$$g_{io}(x) = |i_o^*((k+1)T) - i_o(k+1)| \tag{9}$$

where $v_{C1\_ref}((k+1)T)$ is the reference value of the capacitor voltage, g_{vC1} and g_{io} are the errors associated with the capacitor voltage and load currents, respectively. Based on the multi-objective function, every controlled term in each cost function is evaluated during the numerous possible voltage vectors of the converter as in (1) and (5), where $x \in [0:7]$, [41], [42]. So, g_{vC1} has seven values as well as g_{io}. For each cost function, these seven values are sorted in ascending order from a lower to a higher value. The rank of the capacitor voltage cost function is $r_{\text{vC1}} \in [0:6]$, while the rank of the load currents is $r_{io} \in [0:6]$. For each cost function, the minimum rank refers to the quality of this rank vector if applied. By choosing the minimum ranked vector for each cost function, an optimal value for the control targets to their set-points is achieved. But the minimum rank of g_{vC1} is not the same vector for the rank of g_{io} because they have a different discrete model. So, the best optimal vector is obtained according to averaging the two ranks of each corresponding vectors as:

$$R_{\text{avg}}(x) = \frac{r_{\text{vC1}}(x) + r_{io}(x)}{2} \tag{10}$$

The minimum ranked vector (V_x) is selected to be the optimized switching state that should be applied directly to the converter switches, and thus a minimum total error between the variables and their references could be realized. The flowchart of the overall algorithm is depicted in Fig. 9.

$$V_x = \min_{x\in[0:6]} R_{\text{avg}}(x) \tag{11}$$

An example of the proposed method is given in the next part. The switching vectors of the qZSI converter shown in Table I are seven vectors for the capacitor voltage and the load currents. The prediction load current has seven different values as well as the capacitor voltage. Table II shows the selection process inside the main loop to obtain the optimized switching

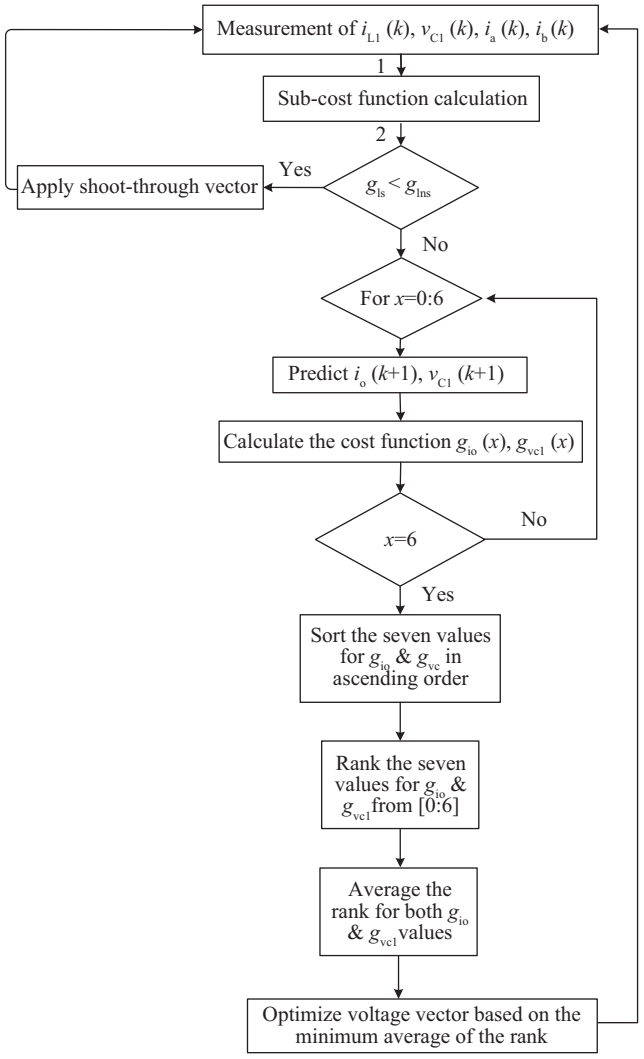

Fig. 9. Flowchart of the proposed algorithm.

TABLE II
RANKING AND SORTING APPROACH

x	V_x	g_{vC1}	g_{io}	r_{vC1}	r_{io}	$R_{avg}(x)$
0	V_0	0.56	2.56	2	3	2.5
1	V_1	1.67	6.77	3	6	4.5
2	V_2	1.80	0.20	4	0	2
3	V_3	0.13	4.76	0	5	2.5
4	V_4	0.50	1.59	1	2	1.5
5	V_5	2.00	2.00	6	4	5
6	V_6	1.90	0.88	5	1	3

vector. Based on the cost function of the capacitor voltage, V_3 has the minimum rank because it has the smallest value. On the other hand, V_5 has the maximum rank value of 6 in the order. Other vectors are ranked according to their values listed in the table. The same procedure is followed with the load current cost functions. In the sixth column of the table, the average rank for each corresponding vector is calculated; for example, for vector V_0, it has rank 2 with load current term and 3 with the capacitor voltage term, so the average rank is 2.5. After averaging all the vector ranks, we can notice that vector V_4 has the minimum average value. So, it will be the optimized vector for qZSI switches, which must be applied in the following sampling time. The maximum value for ranking is decided according to the number of possible switching vectors. More importantly, the rank values should be the same with the load current term and with the capacitor voltage term. By applying the minimum average rank, a minimum total deviation among the two controlled targets is the result. So, they will be as close to their set-point as possible.

V. SIMULATION RESULTS

The whole coding of the proposed FCS-MPC algorithm of qZSI as an m-file is interfaced with the Simulink library to simulate the three-phase qZSI circuit. The used sort and rank algorithm is written and implemented by using the MATLAB script. The MATLAB solver runs at a discrete fixed step of 1 μs at a single-tasking mode. The simulation test was carried out according to the listed parameters in Table III.

TABLE III
PARAMETERS FOR THE QZSI TOPOLOGY IN SIMULATION

Parameter	Symbol	Value
Input voltage	v_{in}	150 V
LC network inductance	$L_1 = L_2 = L$	2 mH
LC network capacitance	$C_1 = C_2 = C$	470 μF
ESR of qZS inductor	R_{ind}	500 mΩ
Load resistance	R	10 Ω/phase
Load inductance	L	15 mH/phase

The load reference power, P_{o_ref}, is stepped up from 1.5 kW to 3 kW at time 0.115 s. According to (3), the peak reference current of the load phase is stepped up from 10 A to 14 A. The reference current for the qZS network inductor will be changed from 6.3 A to 13 A based on the equation (12).

$$i_{L1\_ref} = \frac{P_{o\_ref}}{v_{in}(k)} \tag{12}$$

In this case, the input voltage is assumed to be fixed at a predefined value while the program is running. The maximum load current is at the maximum output power of 3 kW. For the fixed impedance of the load, a peak voltage across the load terminals will result.

To avoid clashes between the DC part and the AC part, and to maintain the regular operation of the qZSI, the reference capacitor voltage, $v_{C1\_ref}((k+1)T)$, must be chosen to be at least twice that of the peak load voltage [32], i.e., at 300 V. In this condition, the maximum voltage of the DC-link voltage, v_i, equals 450 V. For FCS-MPC, the switching frequency of the controlled converter primarily depends on the sampling time, which is chosen as 12 μs. As shown in Fig. 10, which illustrates the Fast Fourier Transform (FFT) spectrum for the load current, the converter is operated nearly at 1 kHz as a switching frequency. The tests conducted to investigate the proposed system are described below.

A. Load Current Step-change

The simulation results of the case study system are shown in Fig. 11. The results in Fig. 11(a) indicate that the inductor current i_{L_1} tracks its reference with very high dynamics. It changed from 6.8 A to 13 A. The actual and reference inductor currents are identical with high dynamic response during

the power step-change. The figure with sampling scaling in Fig. 11(b) shows that the current ripple of the qZSI inductor is 3.5 A (peak-to-peak calculations). Moreover, capacitor voltage remains constant during power change without oscillation and undershoot for the right half-plane phenomena at the output power step interval, as shown in Fig. 11(c). In addition, the voltage ripple of the capacitor has increased after increasing the power, and thus the drawn current is increased. Also, the load currents have changed from 7.5 A to 11 A with a fast response, as depicted in Fig. 11(d). Moreover, the voltage of the DC-link voltage is a pulsated waveform with a peak value

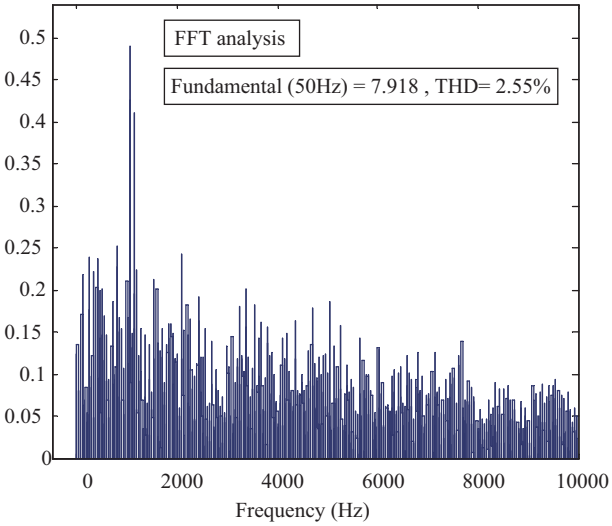

Fig. 10. FFT spectrum for the phase current controlled by the proposed control system.

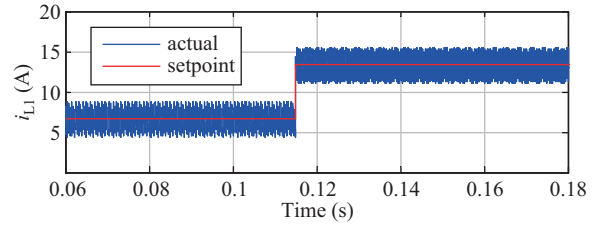

(a) qZSI inductor current i_{L1} and its reference.

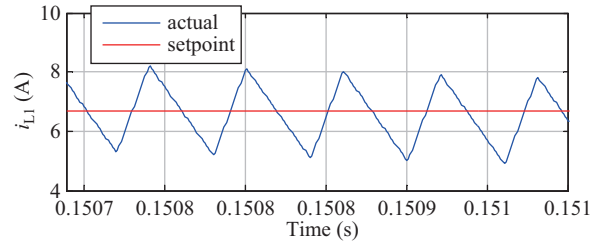

(b) Zoom of the inductor current i_{L1} and its reference.

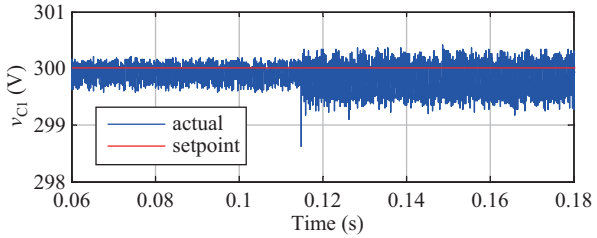

(c) qZSI capacitor voltage v_{C1} and its reference.

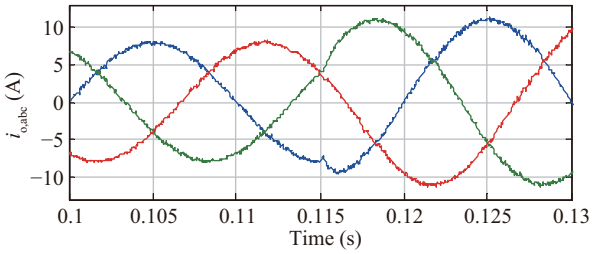

(d) Three-phase load currents

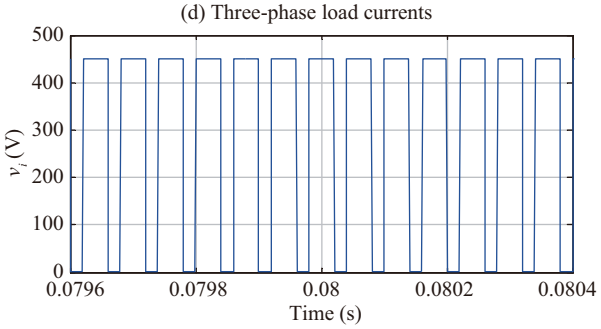

(e) DC-link voltage

Fig. 11. Simulation results for qZSI with the proposed algorithm at load current step-change.

of 450 V (i.e., $2v_{C1}(kT) - v_{in}(kT)$). Also, the shoot-through case (at $v_i = 0$) repeats after two active states (at v_i = 450 V). Thus, the proposed control technique has higher performance in tracking the defined setpoints of the control variables.

B. Frequency Step-change

QZSI has been applied to drive systems [1], so the dynamic performance at different line frequencies is an important test. The results of the simulation at the frequency step-change test are introduced in Fig. 12. The line frequency of the load current has been changed from 50 Hz to 100 Hz. In Fig. 12(a), the inductor current follows its set point at 6.8 A, and the ripple value is constant. Fig. 12(b) shows that the capacitor voltage is still constant at the instant of the frequency change; while in Fig. 12(c), the maximum value of the load current is fixed at 7.5 A after the frequency stepping up. Moreover, the dynamic

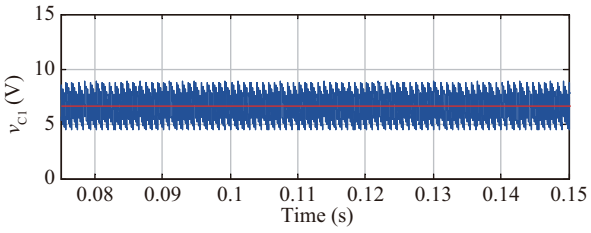

(a) qZSI inductor current i_{L_1} (blue line) and its reference (red line).

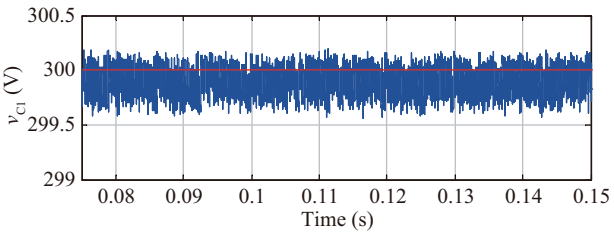

(b) qZSI capacitor voltage (blue line) and its reference (red line).

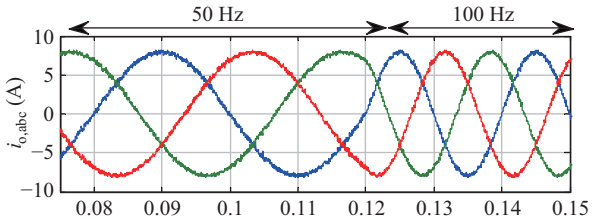

(c) Three-phase load currents, $i_{o,abc}$.

Fig. 12. Simulation results for qZSI with the proposed algorithm at line frequency step-change.

performance of the load current is fast to track the set point of the control action.

VI. Conclusion

This paper aims to improve the design of FCS-MPC with qZSI topology by removing the weighting factor, which needs a complex adjusting process. Using the sub-cost function for the inductor current reduces the calculation burdens and provides a high response in the inductor current to follow the reference value. Both the capacitor voltage and the load currents are controlled using the ranking approach to avoid using the weighting factor. Simulation results have validated the proposed algorithm at different tests.

References

[1] O. Ellabban and H. Abu-Rub, "An overview for the Z-source converter in motor drive applications," *Renewable and Sustainable Energy Reviews*, vol. 61, pp. 537–555, Aug. 2016.

[2] Y. P. Siwakoti, F. Z. Peng, F. Blaabjerg, P. C. Loh, and G. E. Town, "Impedance source networks for electric power conversion Part I: A topological review," *IEEE Transactions on Power Electronics*, vol. 30, no. 2, pp. 699–716, Feb. 2015.

[3] Y. P. Siwakoti, F. Z. Peng, F. Blaabjerg, P. C. Loh, G. E. Town, and S. T. Yang, "Impedance-source networks for electric power conversion Part II: Review of control and modulation techniques," *IEEE Transactions on Power Electronics*, vol. 30, no. 4, pp. 1887–1906, Apr. 2015.

[4] A. Bakeer, M. A. Ismeil, and M. Orabi, "A modified two switched-inductors quasi Z-source inverter," in *Proceedings of 2015 IEEE Applied Power Electronics Conference and Exposition*, 2015, pp. 1693–1699.

[5] F. Gao, P. C. Loh, D. Li, and F. Blaabjerg, "Asymmetrical and symmetrical embedded Z-source inverters," *IET Power Electronics*, vol. 4, no. 2, pp. 181–193, Feb. 2011.

[6] R. Strzelecki, M. Adamowicz, N. Strzelecka, and W. Bury, "New type T-Source inverter," in *Proceedings of 2009 Compatibility and Power Electronics*, 2009, pp. 191–195.

[7] U. S. Ali and V. Kamaraj, "A novel space vector PWM for Z-source inverter," in *Proceedings of the 1st International Conference on Electrical Energy Systems*, 2011, pp. 82–85.

[8] O. Ellabban, J. Van Mierlo, and P. Lataire, "Experimental study of the shoot-through boost control methods for the Z-source inverter," *EPE Journal*, vol. 21, no. 2, pp. 18–29, Jun. 2011.

[9] P. Liu and H. P. Liu, "Permanent-magnet synchronous motor drive system for electric vehicles using bidirectional Z-source inverter," *IET Electrical Systems in Transportation*, vol. 2, no. 4, pp. 178–185, Dec. 2012.

[10] O. Ellabban, J. Van Mierlo, and P. Lataire, "A DSP-based dual-loop peak DC-link voltage control strategy of the Z-source inverter," *IEEE Transactions on Power Electronics*, vol. 27, no. 9, pp. 4088–4097, Sep. 2012.

[11] Y. S. Liu, B. M. Ge, H. Abu-Rub, and F. Z. Peng, "An effective control method for quasi-Z-source cascade multilevel inverter-based grid-tie single-phase photovoltaic power system," *IEEE Transactions on Industrial Informatics*, vol. 10, no. 1, pp. 399–407, Feb. 2014.

[12] J. Rodriguez and P. Cortes, Predictive Control of Power Converters and Electrical Drives, Hoboken:John Wiley & Sons, 2012.

[13] S. Kouro, P. Cortes, R. Vargas, U. Ammann, and J. Rodriguez, "Model predictive control - a simple and powerful method to control power converters," *IEEE Transactions on Industrial Electronics*, vol. 56, no. 6, pp. 1826–1838, Jun. 2009.

[14] P. Cortes, M. P. Kazmierkowski, R. M. Kennel, D. E. Quevedo, and J. Rodríguez, "Predictive control in power electronics and drives," *IEEE Transactions on Industrial Electronics*, vol. 55, no. 12, pp. 4312–4324, Dec. 2008.

[15] P. Cortes, J. Rodriguez, D. E. Quevedo, and C. Silva, "Predictive current control strategy with imposed load current spectrum," *IEEE Transactions on Power Electronics*, vol. 23, no. 2, pp. 612–618, Mar. 2008.

[16] C. L. Xia, T. Liu, T. N. Shi, and Z. F. Song, "A simplified finite-control-set model-predictive control for power converters," *IEEE Transactions on Industrial Informatics*, vol. 10, no. 2, pp. 991–1002, May 2014.

[17] H. A. Young, M. A. Perez, J. Rodriguez, and H. Abu-Rub, "Assessing finite-control-set model predictive control: A comparison with a linear current controller in two-level voltage source inverters," *IEEE Industrial Electronics Magazine*, vol. 8, no. 1, pp. 44–52, Mar. 2014.

[18] J. Böcker, B. Freudenberg, Andrew The, and S. Dieckerhoff, "Experimental comparison of model predictive control and cascaded control of the modular multilevel converter," *IEEE Transactions on Power Electronics*, vol. 30, no. 1, pp. 422–430, Jan. 2015.

[19] O. Ellabban, J. Van Mierlo, and P. Lataire, "Capacitor voltage control techniques of the Z-source inverter: A comparative study," *EPE Journal*, vol. 21, no. 4, pp. 13–24, Dec. 2011.

[20] W. Mo, P. C. Loh, and F. Blaabjerg, "Model predictive control for Z-source power converter," in *Proceedings of the 8th International Conference on Power Electronics - ECCE Asia*, 2011, pp. 3022–3028.

[21] W. Mo, P. C. Loh, Andrew, and F. Blaabjerg, "Model predictive control of Z-source neutral point clamped inverter," in *Proceedings of 2011 IEEE Energy Conversion Congress and Exposition*, 2011, pp. 3838–3843.

[22] M. Wei, A. P. C. Loh, and B. Frede, "Maximum power point tracking technique implementation of Z-source inverter through finite step model predictive control strategy," in *Proceedings of the 7th IEEE Conference on Industrial Electronics and Applications*, 2012, pp. 1523–1528.

[23] M. Mosa, O. Ellabban, A. Kouzou, H. Abu-Rub, and J. Rodríguez, "Model predictive control applied for quasi-Z-source inverter," in *Proceedings of the Twenty-Eighth Annual IEEE Applied Power Electronics Conference and Exposition*, 2013, pp. 165–169.

[24] O. Ellabban, M. Mosa, H. Abu-Rub, and J. Rodríguez, "Model predictive control of a grid connected quasi-Z-source inverter," in *Proceedings of 2013 IEEE International Conference on Industrial Technology*, 2013, pp. 1591–1596.

[25] M. Mosa, H. Abu-Rub, and J. Rodriguez, "High performance predictive control applied to three phase grid connected quasi-Z-source inverter," in *Proceedings of the 39th Annual Conference of the IEEE Industrial Electronics Society*, 2013, pp. 5812–5817.

[26] M. Mosa, G. M. Dousoky, and H. Abu-Rub, "A novel FPGA implementation of a model predictive controller for sic-based quasi-Z-source inverters," in *Proceedings of 2014 IEEE Applied Power Electronics Conference and Exposition*, 2014, pp. 1293–1298.

[27] M. Mosa, R. S. Balog, and H. Abu-Rub, "High-performance predictive control of quasi-impedance source inverter," *IEEE Transactions on Power Electronics*, vol. 32, no. 4, pp. 3251–3262, Apr. 2017.

[28] S. A. Davari and D. A. Khaburi, "Using predictive control and q-ZSI to drive an induction motor supplied by a PV generator," in *Proceedings of the 5th Annual International Power Electronics, Drive Systems and Technologies Conference*, 2014, pp. 61–65.

[29] A. Bakeer, M. A. Ismeil, M. Orabi, and R. Kennel, "Control of switched-inductor quasi Z-source inverter (SL-qZSI) based on model predictive control technique (MPC)," in *Proceedings of 2015 IEEE International Conference on Industrial Technology*, 2015, pp. 2248–2253.

[30] A. Bakeer, M. A. Ismeil, A. Kouzou, and M. Orabi, "Development of MPC algorithm for quasi Z-source inverter (qZSI)," in *Proceedings of the 3rd International Conference on Control, Engineering & Information Technology*, Tlemcen, Algeria, 2015, pp. 1–6.

[31] A. Bakeer, M. A. Ismeil, and M. Orabi, "Simple cost function and low calculations MPC algorithm for qZSI," in *Proceedings of 2015 IEEE International Telecommunications Energy Conference*, 2015, pp. 1–6.

[32] A. Bakeer, M. A. Ismeil, and M. Orabi, "A powerful finite control set-model predictive control algorithm for quasi Z-source inverter," *IEEE Transactions on Industrial Informatics*, vol. 12, no. 4, pp. 1371–1379, Aug. 2016.

[33] A. Ayad, P. Karamanakos, and R. Kennel, "Direct model predictive current control of quasi-Z-source inverters," in *Proceedings of 2015 IEEE International Symposium on Predictive Control of Electrical Drives and Power Electronics*, 2015, pp. 62–72.
[34] A. Ayad and R. Kennel, "Direct model predictive control of quasi-Z-source inverter compared with the traditional PI-based PWM control," in *Proceedings of the 17th European Conference on Power Electronics and Applications*, 2015, pp. 1–9.
[35] A. Ayad, P. Karamanakos, and R. Kennel, "Direct model predictive current control strategy of quasi-Z-source inverters," *IEEE Transactions on Power Electronics*, vol. 32, no. 7, pp. 5786–5801, Jul. 2017.
[36] Y. S. Liu, B. M. Ge, H. Abu-Rub, H. X. Sun, F. Z. Peng, and Y. S. Xue, "Model predictive direct power control for active power decoupled single-phase quasi-Z-source inverter," *IEEE Transactions on Industrial Informatics*, vol. 12, no. 4, pp. 1550–1559, Aug. 2016.
[37] S. Bayhan, M. Trabelsi, and H. Abu-Rub, "Model predictive control of Z-source four-leg inverter for standalone photovoltaic system with unbalanced load," in *Proceedings of 2016 IEEE Applied Power Electronics Conference and Exposition*, 2016, pp. 3668–3668.
[38] S. Bayhan, H. Abu-Rub, and R. S. Balog, "Model predictive control of quasi-Z-source four-leg inverter," *IEEE Transactions on Industrial Electronics*, vol. 63, no. 7, pp. 4506–4516, Jul. 2016.
[39] S. Bayhan and H. Abu-Rub, "Model predictive control of quasi-Z source three-phase four-leg inverter," in *Proceedings of the 41st Annual Conference of the IEEE Industrial Electronics Society*, 2015, pp. 362–367.
[40] P. Cortes, S. Kouro, B. La Rocca, R. Vargas, J. Rodriguez, J. I. Leon, S. Vazquez, and L. G. Franquelo, "Guidelines for weighting factors design in model predictive control of power converters and drives," in *Proceedings of 2019 IEEE International Conference on Industrial Technology*, 2009, pp. 1–7.
[41] C. A. Rojas, J. Rodriguez, F. Villarroel, J. R. Espinoza, C. A. Silva, and M. Trincado, "Predictive torque and flux control without weighting factors," *IEEE Transactions on Industrial Electronics*, vol. 60, no. 2, pp. 681–690, Feb. 2013.
[42] F. Villarroel, J. Espinoza, C. Rojas, C. Molina, and E. Espinosa, "A multiobjective ranking based finite states model predictive control scheme applied to a direct matrix converter," in *Proceedings of the 36th Annual Conference on IEEE Industrial Electronics Society*, 2010, pp. 2941–2946.

Abualkasim Bakeer (S'14) received the B.Sc. and M.Sc. (Hons.) degrees in Electrical Engineering from Aswan University, Egypt, in 2012 and 2017, respectively. Beginning in 2014, he joined the Electrical Engineering Department, Faculty of Engineering, Aswan University, Aswan, Egypt, first as a demonstrator, and then as an assistant lecturer in 2017. Beginning in September 2019, he began working toward a Ph.D. degree with the Department of Electrical Power Engineering and Mechatronics, Tallinn University of Technology, Estonia. He is the author/co-author of more than 20 scientific papers. He serves as a reviewer for the IEEE Transaction on industrial electronics, IEEE Transactions on industrial informatics, and IEEE Journal of Emerging and Selected Topics in Industrial Electronics. His main research interests include focusing on DC-DC converters, fault diagnosis and fault tolerance, AC drives, impedance-source power converters, and model predictive control. Mr. A. Bakeer has been a member of the Power Electronics Society (PELS), Industrial Electronics Society (IES) since 2020.

Gaber Magdy received the B.Sc. and M.Sc. (Hons.) degrees in Electrical Engineering from Aswan University, Egypt, in 2011 and 2014, respectively, and the jointly supervised Ph.D. degree in Electrical Engineering from Minia University, Egypt (Main university), and Kyushu Institute of Technology, Japan (Host university), in 2019. He joined the Electrical Engineering Department, Faculty of Energy Engineering, Aswan University, Aswan, Egypt, first as a Demonstrator (Assistant Researcher) in December 2011, and then became an Assistant Lecturer in November 2014. From 2017 to 2019, he was a researcher in the Department of Electrical and Electronic Engineering, Kyushu Institute of Technology, Japan. He is currently an assistant professor at the Department of Electrical Engineering, Faculty of Energy Engineering, Aswan University, Aswan, Egypt. His research interests include power system stability, dynamics, and control, digital control, smart/micro-grid control, renewable energies, and energy storage systems.

Andrii Chub (S'12–M'17–SM'19) received the B.Sc. and M.Sc. degrees from Chernihiv State Technological University, Chernihiv, Ukraine, in 2008 and 2009, respectively. In 2016, he received a Ph.D. degree in Electrical Engineering from Tallinn University of Technology, Estonia. He is a Senior Researcher at the Power Electronics Group, TalTech, Estonia. He was a Visiting Research Fellow at Kiel University in 2017 and a Postdoctoral Researcher at Federico Santa Maria Technical University between 2018 and 2019. He has co-authored over 100 papers and book chapters on power electronics and applications. In addition, he holds several patents and utility models. He received numerous best paper awards at IEEE conferences and the 2018 Industrial Electronics Society Best Conference Paper Award. His research interests include DC-DC converters, DC microgrids, renewable energy conversion systems for energy-efficient residential buildings, fault tolerance and reliability in power electronic systems. Dr. Chub is an Associate Editor of the IEEE Journal of Emerging and Selected Topics in Industrial Electronics.

Dmitri Vinnikov received the Dipl.Eng., M.Sc., and Ph.D.Sc.techn. degrees in Electrical Engineering from Tallinn University of Technology (Estonia) in 1999, 2001, and 2005, respectively. He is the Head of the Power Electronics Group, Department of Electrical Power Engineering and Mechatronics, Tallinn University of Technology. He has authored or coauthored two books, five monographs and one book chapter as well as more than 200 published papers on power converter design and development and is the holder of numerous patents and utility models in this field. His research interests include applied design of power electronic converters and control systems, renewable energy conversion systems (photovoltaic and wind), impedance-source power converters, and implementation of wide bandgap power semiconductors. D. Vinnikov is a Senior Member of the IEEE and Chair of the IES/PELS Joint Societies Chapter of the IEEE Estonia Section.